

Revue des Composites et des Matériaux Avancés-Journal of Composite and Advanced Materials

Vol. 35, No. 5, October, 2025, pp. 885-891

Journal homepage: http://iieta.org/journals/rcma

Some Properties of (NiO)_{1-x}(Co₃O₄)_x Nano Composite Thin Films Prepared by Chemical Spray Pyrolysis for Photodetector Application



Huda R. Abdulridha Mohammed* Nahida B. Hasan, Mohammed Hadi Shinen

Department of Physics, College of Science, University of Babylon, Hillah 51002, Iraq

Corresponding Author Email: huda.mohammed@student.uobabylon.edu.iq

Copyright: ©2025 The authors. This article is published by IIETA and is licensed under the CC BY 4.0 license (http://creativecommons.org/licenses/by/4.0/).

https://doi.org/10.18280/rcma.350508

Received: 8 September 2025 Revised: 16 September 2025 Accepted: 19 October 2025 Available online: 31 October 2025

Keywords:

composite thin films, optical constants, electrical properties, photodetector

ABSTRACT

Spray pyrolysis was utilized to create $(NiO)_{1-x}(Co_3O_4)_x$ composite thin films on a glass substrate using 0.05 M NiCl₂·6H₂O and 0.05 M CoCl₂·6H₂O dissolved in distilled water. The refractive index, reflectivity, and real and imaginary dielectric constants all rose as the concentration of Co₃O₄ increased. This may be due to the homogeneity and surface roughness of the films, a result that is beneficial for Photodetector applications. The electrical properties include D.C conductivity studied. The results show that the prepared films have two activation energies (Ea1, Ea2). The photodetector devices were evaluated at (380–620) nm. These devices showed steady current across numerous cycles and great repeatability and stability. Calculated merit statistics included (responsivity) (R λ), specific detectivity (D*), external quantum efficiency (EQE), photosensitivity (ξ), and noise equivalent power (NEP). The (NiO)₂₅(Co₃O₄)₇₅ films showed excellent performance in UV and green light. The (NiO)₇₅(Co₃O₄)₂₅ films showed the highest response in red. Pure Co₃O₄ showed good response to blue light. Therefore, changing the ratio of NiO to Co₃O₄ allows the films to be tailored to the optical spectrum, making them suitable for various photodetection applications depending on the target wavelength.

1. INTRODUCTION

Semiconductors have distinct properties when compared to other materials, and their ability to be doped with various types and concentrations of impurities to vary their resistivity is one of their most important properties. Semiconductors are sensitive to electric and magnetic fields because their physical properties change as they increase in temperature, light, and doping, which allows them to control their properties [1]. Because of the very low free electrons and holes concentration, its conductance is typically much lower than that of a metal. It is also strongly dependent on temperature, increasing rapidly with an increase in temperature because the probability of thermal excitation increases with temperature. Of course, the conductance of a semiconductor is a function of the energy gap. Semiconductor crystals have two types: n-type and p-type [2].

NiO can be made in a variety of ways. NiO is produced when nickel powder combines with oxygen when heated above 400°C [3, 4]. Green nickel oxide is produced in certain commercial methods by heating a combination of nickel powder and water to 1000°C; adding NiO can speed up this reaction [5-7]. Cobalt oxide is one of the nanomaterials that are used to treat cancer because of its important properties such as biocompatibility, stability, drug packaging and quality. Nano-tools have been used to improve and develop delivery agents and effects of chemotherapy directly to cancer cells, to

reduce the toxic effect on healthy living tissues while maintaining the fight against tumors efficiently [8-10]. Because of the toxic properties of Co₃O₄ nanoparticles used to facilitate the treatment of cancerous liver cells, cobalt oxide, which has a high magnetic moment, is currently used as a hybrid compound, and individually combined for medical purposes. Currently, these compounds have been used in several areas, from industry to medicine, when the size of these compounds is nanoscale [11-14].

In this study, the spray pyrolysis technique was used to make thin films of the composite (NiO)_{1-x}(Co₃O₄)x. These two materials NiO and Co₃O₄ were used due to their good optical properties, and this technique was also used to find homogeneous nano-films for Photodetector Application.

2. EXPERIMENTAL

Spray pyrolysis was used to create the (NiO)_{1-x}(Co₃O₄)_x composite thin films on a glass substrate. The spraying solution was prepared from 0.05 M of NiCl₂·6H₂O and 0.05 M of CoCl₂·6H₂O dissolved in 100 ml distilled water. (NiO)_{1-x}(Co₃O₄)_x composite prepared with various concentration (0, 25, 50, 75, 100)%. Deposition parameters: hold time of 2 minutes and distance between nozzle and substrate of 30 cm.

Table 1 shows the volumetric ratios of the solutions.

Table 1. Volumetric ratios of the solutions used in the preparation of thin films

Sample	Solution of NiCl ₂ ·6H ₂ O	Solution of CoCl ₂ ·6H ₂ O		
NiO pure	100%	0%		
(NiO) ₇₅ (Co ₃ O ₄) ₂₅	75%	25%		
(NiO) 50(Co ₃ O ₄)50	50%	50%		
(NiO) ₂₅ (Co ₃ O ₄) ₇₅	25%	75%		
Co ₃ O ₄ pure	0%	100%		

3. RESULTS AND DISCUSSION

3.1 Optical constants

3.1.1 The absorption coefficient (α)

The absorption coefficient (α) of composite thin films are calculated using Eq. (1). The absorption coefficient is determined from the region of high absorption at the fundamental absorption edge of the film. The variation of the absorption coefficient versus wavelength for (NiO)_{1-x}(Co₃O₄)_x composite thin films with different ratios of Co₃O₄ (25, 50, 75 and 100) wt.%, are presented in Figure 1.

$$\alpha = \frac{2.303 \times A}{t} \tag{1}$$

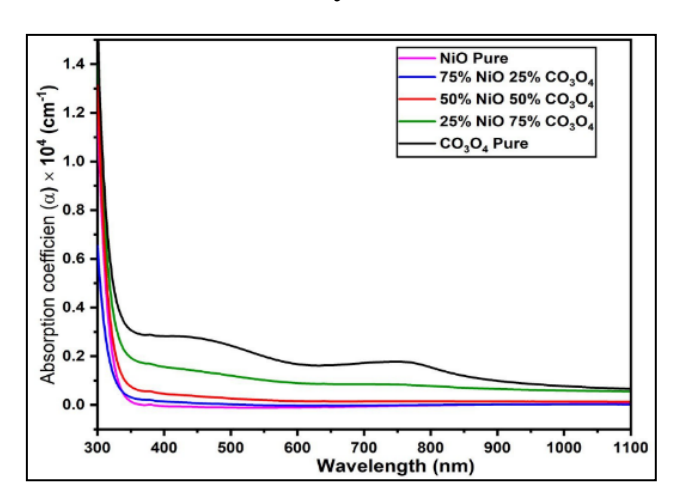


Figure 1. The absorption coefficient spectra for composite thin films at varying volumes of (x)

The figures show that the absorption coefficient is increased with increasing ratios of Co₃O₄ due to the absorption coefficient being directly proportional to the absorbance according to the relationship [15].

3.1.2 The transmittance spectra

The transmittance spectra of $(NiO)_{1-x}(Co_3O_4)_x$ composite thin films are shown in Figure 2.

Figure 2 shows the transmittance spectra decreasing with increasing concentration of the $\mathrm{Co_3O_4}$. This could be attributed to a rise in film homogeneity and surface roughness. The decline in transmittance behavior might also be attributed to a rise in doped atoms, increasing collisions between the atoms, and incident photons, which is in line with the findings of the study [16]. The $\mathrm{Co_3O_4}$ thin film has two absorption edges, at low and high energies. which is due to the presence of 2

different cobalt ions Co^{+2} and Co^{+3} . So, the firstenergy gap at low energies corresponds to the charge transfer process O^{-2} to Co^{+2} , and the second energy gap at high energies corresponds to the charge transfer process O^{-2} to Co^{+3} .

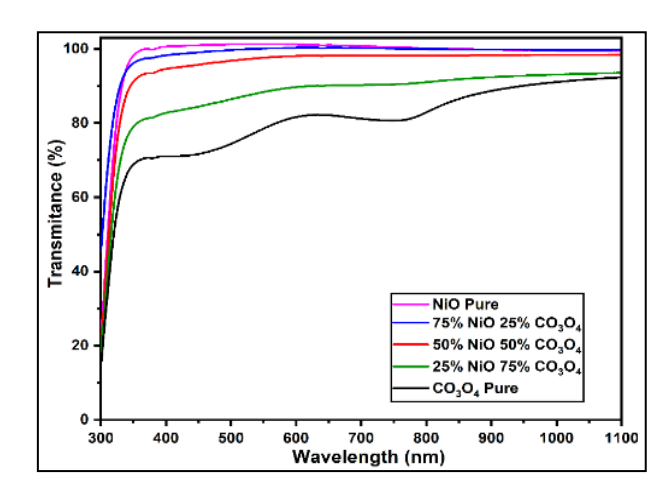


Figure 2. Spectrum of transmittance for composite thin films at varying percentages of (x)

3.1.3 The reflectance spectrum

Figure 3 displays the reflectance of composite thin films. According to this figure, the reflectance rises as the Co₃O₄ concentration does, which is in line with the researchers' findings [17].

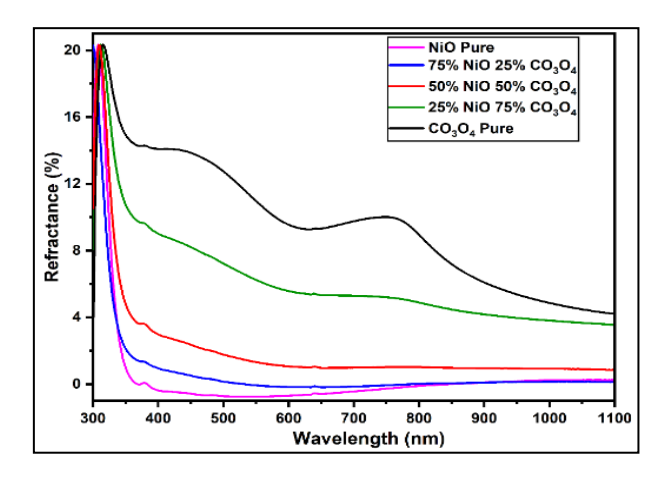


Figure 3. Reflectance spectrum for composite thin films of at varying volumes of (x)

3.1.4 The real and imaginary dielectric constant's

According to the dielectric constant's real (ϵ 1) and imaginary (ϵ 2) components are written as follows [18]:

$$\varepsilon_1 = n^2 - k^2 \tag{2}$$

$$\varepsilon_2 = 2nk$$
 (3)

where.

(k): is the extinction coefficient and;

(n): is the refractive index.

The imaginary part quantifies the rate of wave dissipation in the medium, whereas the real (ϵ_1) component is associated with dispersion. Figures 4 and 5 show the real and imaginary dielectric constants. Based on these figures, the values of ϵ_1 and ϵ_2 increase with increasing wavelength [19].

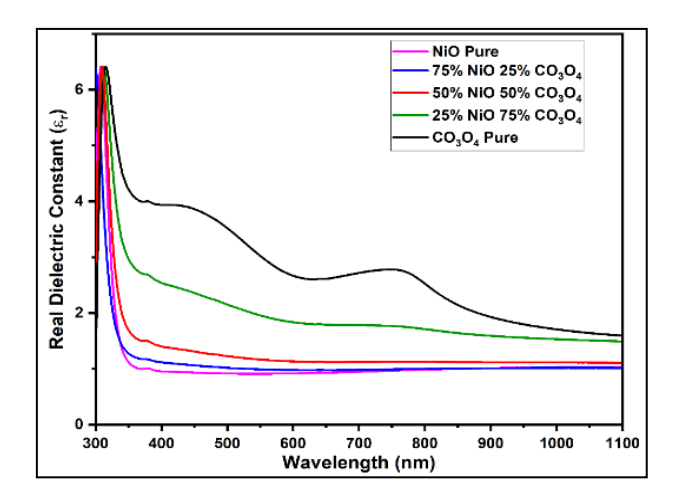


Figure 4. The dielectric constant spectrum's real component for composite thin films at varying voltage percentages of (x)

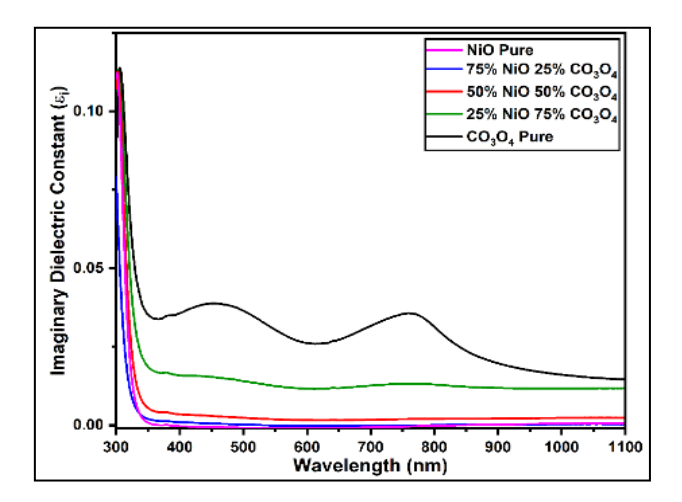


Figure 5. The dielectric constant spectrum's imaginary component for composite thin films at various vol.% of (x)

3.2 Electrical properties

3.2.1 D.C conductivity

The D.C Conductivity $(\sigma_{d.c})$ of the film depends upon several factors such as the preparation method, and the preparation environments. It has been studying the dependence of D.C conductivity $(\sigma_{d.c})$ on different ratio.

In the semiconductor granular borders are of great importance in the mobility of charge carriers because grain boundaries are high-density areas of defects, it's possible to be centers for scattering (scattering centers), centers for capture or trapping centers or centers for the union of charge carriers (recombination centers). In all these cases, the defects and

impurities and grain boundaries have a direct impact on the mobility of charge carriers, then on conductivity [20].

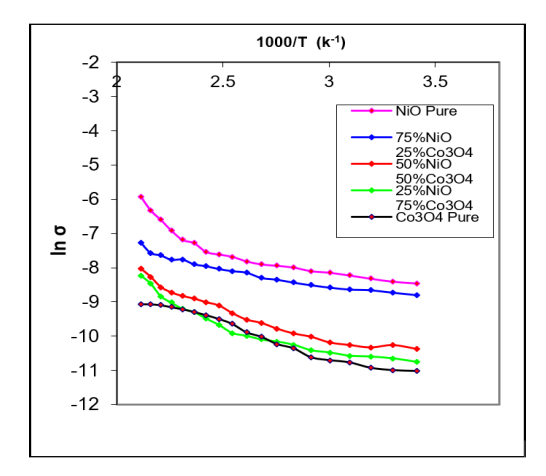


Figure 6. The variation of Lnσ with 1000/T for the prepared thin films

Figure 6 shows the variation of Lno with inverted absolute temperature 1000/T, the electrical activation energy Ea₁ and Ea₂ for the (NiO)_{1-x}(Co₃O₄)_x films was calculated. The results of Ea₁ and Ea₂ listed in Table 2 show that the activation energy (Ea₁ and Ea₂) decreases with increasing Co₃O₄ ratios and this corresponds with the results of the optical properties as impurities increase, leading to a decrease in the optical energy gap [21].

The plot displays how the DC conductivity (ln σ) of different compositions of thin films varies with temperature. This relationship helps in determining the activation energy Ea. All curves decrease with increasing 1000/T (i.e., with decreasing temperature), indicating typical semiconducting behavior. Activation energy can be calculated from the slope increasing Co₃O₄ content decreases the conductivity, possibly due to structural changes or increased grain boundary resistance.

3.2.2 Hall effect

The Hall coefficient (RH), carrier concentrations (n), electrical conductivity (σ), and Hall mobility (μ H), have been determined in Table 3. Hall coefficient (RH) can be calculated from Eq. (4) [22].

$$R_{\rm H} = \frac{V_{\rm H}}{I} \cdot \frac{t}{B} \tag{4}$$

It's important to know the electrical properties. From the measurements we find that the RH value is positive, that means all the films is p-type and the majority charge are holes.

Table 2. DC conductivity and activation energy for the prepared thin films

Samples	ρ (Ω.cm) at R.T	σ = 1/ρ (Ω.cm) ⁻¹ at R.T	Ea ₁ (eV)	Temp. Range (K)	Ea ₂ (eV)	Temp. Range (K)
NiO Pure	2162.4	4.625 E-04	0.080294	(293-400)	0.097362	(400-473)
NiO 75 C ₀₃ O ₄ 25	3277.6	3.051 E-04	0.066140	(293-400)	0.090241	(400-473)
NiO 50 Co ₃ O ₄ 50	11281.2	8.864E-05	0.062330	(293-400)	0.072847	(400-473)
NiO 25 Co ₃ O ₄ 75	20175.6	4.957E-05	0.050102	(293-400)	0.066005	(400-473)
Co ₃ O ₄ Pure	15436	6.478E-05	0.039800	(293-400)	0.063561	(400-473)

Table 3. Hall effect characterization for prepared thin films

Samples	R _H (cm ³ /c)	n _H (1/cm ³)	$\sigma_{R.T}(\Omega.cm)^{-1}$	ρ R.T (Ω.cm)	μ (cm ² /V.s)
NiO Pure	1.213E+11	5.145E+07	6.955E-08	1.438E+07	8.43E+03
NiO 75 Co ₃ O ₄ 25	2.500E+07	2.50E+11	9.402E-06	1.064E+05	2.35E+02
NiO 50 Co ₃ O ₄ 50	5.567E+06	1.121E+12	3.580E-04	2.793E+03	1.993E+03
NiO 25 Co ₃ O ₄ 75	1.408E+09	4.43E+09	1.860E-10	5.372E+09	2.62E-01
Co ₃ O ₄ Pure	1.470E+06	4.248E+12	9.859E-06	1.014E+05	1.449E+01

Table 3 shows that the Hall coefficient decreases with increasing mixing ratios. We also note that conductivity and the concentration of charge carriers increase with increasing impurity ratios. This is attributed to the increased concentration of charge carriers, which leads to a shrinkage of the region between the Fermi level and the conductivity edge. This, in turn, leads to a decrease in activation energy with increasing mixing ratios. The concentration of charge carriers also depends on the crystalline microstructure and surface chemical interactions [23].

3.3 Photodetector

The sensitivity (S) is used to know the increase in the current in a sample under illumination. Conductivity rises when the light is turned on, and after it is turned off, the current returns to its original rate. This process is repeated many times [24, 25].

The current versus time (I-t) graph of the photodetector device is shown in Figures 7-10. Power intensities of 6.17, 5.61, 10.38, and 5.11 mW/cm² were used to evaluate the device at wavelengths of 380, 460, 520, and 620nm. There was no bias voltage applied during these experiments. The device showed outstanding repeatability and stability by maintaining a constant current throughout several cycles. The ratio of the incident optical power at a certain wavelength to the output electrical signal is known as photoresponsivity (R_{λ}) [26].

$$R_{\lambda} = I_{\text{photo}} / P_{\text{in}} S \tag{5}$$

Iphoto stands for the generated photocurrent, S for the photodetector's active area, and Pin for the intensity of incident light or radiation. The ratio of the number of charge carriers a device produces to the number of phoor η . S is the active region of the photodetector, Pin is the intensity of the incident light or radiation, and Iphoto is the generated photocurrent. External quantum efficiency, or η , is the ratio of the number of charge carriers generated by a device to the number of photons striking it. It sheds light on how well photodetectors transform photons into different types of charge carriers. The phrase describes the percentage of holes or electrons that undergo transformation as a result of photons being stimulated by an energy source. The following equations are used to accomplish the evaluation [27, 28]:

$$EQE(\eta) = I_{photo} / P_{in} S \times hc/q\lambda \times 100\%$$
 (6)

$$EQE(\eta) = R \times hc/q\lambda \times 100\%$$
 (7)

where, q is the unit of electric charge, c is the velocity of light, and h is the Planck constant. The photosensitivity is calculated by dividing the dark current by the quotient of the current change (ΔI) [29]:

$$\xi = I_{\text{photo}} - I_{\text{dark}} / I_{\text{dark}}$$
 (8)

Specific detectivity (D*) of photodetector refers to its capacity to detect low-intensity signals given by [30]:

$$D^* = \sqrt{sf}/NEP \tag{9}$$

where, f is the bandwidth, the acronym NEP stands for noise equivalent power. It is appraised.

$$NEP = i_n/R \tag{10}$$

where, in represents the dark current noise.

The table above shows the spectral measurements of thin films composed of NiO and Co₃O₄ with different compositions, when exposed to different wavelengths (380, 460, 520, and 620 nm). The table contains several important parameters for evaluating the performance of the films as photodetectors. Interpretation of the results by wavelength.

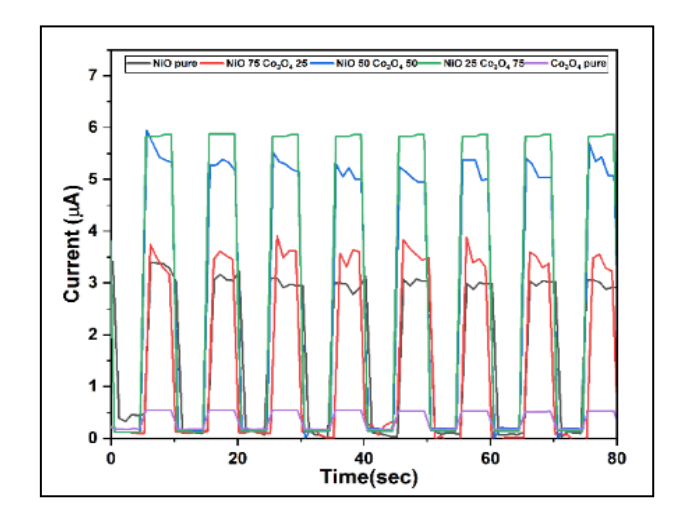


Figure 7. Photo response time of prepared for composite thin films at wavelength 620 nm (red light)

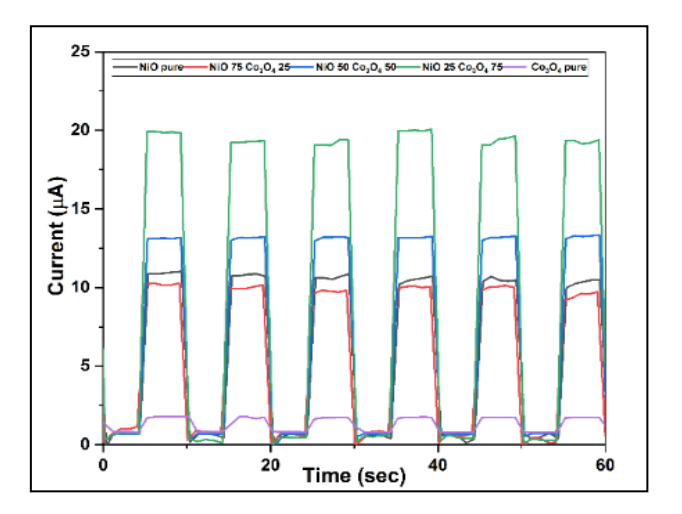
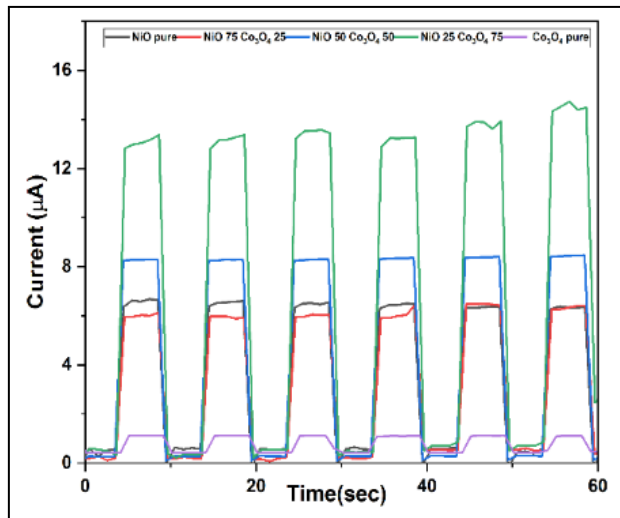


Figure 8. Photo response time of prepared for composite thin films at 460 nm (blue light)





NiO 75 Co.O. 25

60

50

Current (µA) 8 6

20

10

0 -

NiO 50 Co.O. 50

NiO 25 Co.O. 75

Table 4. Spectral measurements for composite thin films measured at (380, 460, 520 and 620) illumination

		U.V L	ight (380 nm)		
Sample	Rλ A/W	η(λ)%	$NEP \times 10^{-11} \text{ W} \cdot \text{Hz}^{1/2}$	$D^* \times 10^9$ (cm·Hz ^{1/2} ·W ⁻¹)	S%
NiO Pure	3.40	11.080	3.45	7.33	1466.716
NiO ₇₅ Co ₃ O _{4 25}	4.95	16.154	1.59	1.59	4697.571
NiO ₅₀ Co ₃ O ₄ ₅₀	1.33	4.355	5.92	4.28	1212.754
NiO ₂₅ Co ₃ O ₄ 75	6.23	20.325	1.84	1.37	5987.539
Co ₃ O ₄ Pure	5.01	1.635	2.33	1.09	153.948
		Blue L	ight (460 nm)		
Sample	$R\lambda \times 10^{\text{-3}} \text{ A/W}$	$\eta(\lambda)\%$	NEP × 10^{-11} W·Hz ^{1/2}	$D^* \times 10^9$ (cm·Hz ^{1/2} ·W ⁻¹)	S%
NiO Pure	0.015	4.28	6.69	3.90	834.108
NiO ₇₅ Co ₃ O _{4 25}	1.60	4.30	7.92	3.30	565.265
NiO ₅₀ Co ₃ O ₄ ₅₀	2.19	5.91	4.88	5.35	1166.293
NiO ₂₅ Co ₃ O ₄ 75	2.69	7.25	4.42	5.92	1176.459
Co ₃ O ₄ Pure	3.62	9.77	3.36	7.77	71.689
		Green 1	Light (520 nm)		
Sample	$R\lambda \times 10^{-3} \ A/W$	$\eta(\lambda)\%$	NEP × 10 ⁻¹¹ W·Hz ^{1/2}	$D^* \times 10^9$ (cm·Hz ^{1/2} ·W ⁻¹)	S%
NiO Pure	5.97	1.42	2.17	1.09	217.539
NiO ₇₅ Co ₃ O _{4 25}	2.05	4.89	7.01	3.39	3348.369
NiO ₅₀ Co ₃ O ₄ ₅₀	6.56	1.56	8.21	2.89	2196.371
NiO ₂₅ Co ₃ O _{4 75}	9.88	23.55	4.33	5.48	16484.565
Co ₃ O ₄ Pure	1.65	0.39	6.71	3.54	176.304
		Red L	ight (620 nm)		
Sample	$R\lambda \times 10^{\text{-3}} \text{ A/W}$	$\eta(\lambda)\%$	NEP × 10 ⁻¹¹ W·Hz ^{1/2}	$D^* \times 10^9$ (cm·Hz ^{1/2} ·W ⁻¹)	S%
NiO Pure	4.66	1.73	1.86	1.40	136.878
NiO ₇₅ Co ₃ O _{4 25}	8.74	9.47	3.48	7.50	8128.375
NiO ₅₀ Co ₃ O ₄ ₅₀	2.52	5.03	2.37	1.10	4202.252
NiO ₂₅ Co ₃ O _{4 75}	1.14	2.27	1.11	2.35	419.843
Co ₃ O ₄ Pure	2.94	0.58	4.17	6.27	34.275

A-Under UV (380 nm), the highest efficiency (η) = 20.3% was for the 75% NiO - 25% Co₃O₄ sample. The highest spectral response (R λ) = 6.23 A/W was for the same sample. This indicates that the introduction of 25% Co₃O₄ to NiO significantly improved the photoelectric performance in UV (Table 4).

B-Blue Light (460 nm), we observe that performance improves with increasing Co_3O_4 , with the highest $R\lambda = 3.62\times10^{-3}$ A/W and $\eta = 9.77\%$ for the pure Co_3O_4 sample. Co_3O_4 appears to be more suitable for blue light than NiO.

C-Green Light (520 nm), The 75% NiO - 25% Co₃O₄

sample showed the highest response (η = 23.55%, R λ = 9.88 × 10⁻³ A/W). This indicates that this combination is very effective for green light.

D-Red Light (620 nm), We observe the best performance for the 25% Co_3O_4 - 75% NiO sample (R λ = 8.74×10⁻³ A/W). While pure Co_3O_4 showed a weak response at this wavelength, we conclude that changing the ratio of NiO to Co_3O_4 allows the films to adjust their spectral response, making them suitable for various photodetection applications depending on the target wavelength.

The demonstrated effective charge separation capabilities,

responsivity, and sensitivity make this heterostructure an exciting choice for detector applications. These results are promising for the development of next generation optoelectronic de-vices, such as hybrid or dye sensitized solar cells, ultra-violet and visible detectors.

4. CONCLUSIONS

Using 0.05 M of NiCl₂·6H₂O and 0.05 M of CoCl₂·6H₂O diluted in distilled water, the chemical spray pyrolysis approach has successfully produced the composite thin films. This could be because the films become more homogeneous and rougher on the surface, which makes them appropriate for Photodetector. Electrical Properties the films were found to be p-type with two activation energies (Ea₁ and Ea₂). Photodetector Performance, the (NiO)25(Co₃O₄)75 films showed excellent performance in UV and green light and changing the ratio of NiO to Co₃O₄ allows the films to be tailored to the optical spectrum, making them suitable for various photodetection applications depending on the target wavelength.

ACKNOWLEDGMENT

The Department of Physics, College of Science, University of Babylon, Iraq, is gratefully acknowledged by the authors.

REFERENCES

- [1] Fujii, E., Tomozawa, A., Torii, H.T.H., Takayama, R.T.R. (1996). Preferred orientations of NiO films prepared by plasma-enhanced metalorganic chemical vapor deposition. Japanese Journal of Applied Physics, 35(3A): L328. https://doi.org/10.1143/JJAP.35.L328
- [2] Sato, H., Minami, T., Takata, S., Yamada, T. (1993). Transparent conducting p-type NiO thin films prepared by magnetron sputtering. Thin Solid Films, 236(1-2): 27-31. https://doi.org/10.1016/0040-6090(93)90636-4
- [3] Viguie, J.C., Spitz, J. (1975). Chemical vapor deposition at low temperatures. Journal of the Electrochemical Society, 122(4): 585. https://doi.org/10.1149/1.2134266
- [4] Slewah, G. (1990). Study of electrical and optical properties of thin film of CdS and CdS: In prepared by spray pyrolysis technology, Doctoral dissertation, College of Sciences, University of Basrah.
- [5] Ramsay, D. (1976). The role of substrates in the growth of self-supporting thin films. In Proceedings of the 1974 annual conference of the Nuclear Target Development Society.
- [6] Patnaik, P. (2003). Handbook of Inorganic Chemicals. New York: McGraw-Hill.
- [7] Greenwood, N.N., Earnshaw, A. (2012). Chemistry of the Elements. Elsevier.
- [8] Lascelles, K., Morgan, L.G., Nicholls, D., Beyersmann, D. (2000). Nickel compounds. Ullmann's Encyclopedia of Industrial Chemistry. https://doi.org/10.1002/14356007.a17 235.pub2
- [9] Khalaf, A.J., Hasan, N.B. (2020). Investigation and prepared of [Cu. sub. 2] ZnSn [S. sub. 4] compound films as a gas sensor by pulse laser deposition. Neuroquantology, 18(1): 117-124.

- https://doi.org/10.14704/nq.2020.18.1.NQ20116
- [10] Hassan, N.B., Ghazi, R.A. (2016). Optoelectronic Properties of Detector (p-Cd1-xZnxS/n-Si) Preparing by Spray Pyrolysis Technique.
- [11] Alfayhan, A.S., Hasn, N.B. (2024). Influence of pulse laser deposition on the structural and optical properties of CZTS for sensor applications. Revue des Composites et des Matériaux Avancés, 34(1): 95. https://doi.org/10.18280/rcma.340112
- [12] Mohammad, E.A., Hasan, N.B., Shinen, M.H. (2018). Optical properties of pure P3HT doped with multiwall carbon nanotubes films. Journal of Engineering and Applied Sciences, 13(23): 9994-10000. https://doi.org/10.3923/jeasci.2018.9994.10000
- [13] Kadhim, A.H., Hasan, N.B. (2019). Structural and morphological properties of Fe2O3 and TiO2: Fe2O3 thin films prepared by spray pyrolysis technique. Journal of Kufa-Physics, 11(1): 27-34. http://doi.org/10.31257/2018/JKP/2019/110105
- [14] Mohammed, H.R.A., Al-Ogaili, A.O.M., Abass, K.H. (2023). Structural and dispersion parameters of nanolayers prepared from Al-Ni-Cr alloy. Materials Today: Proceedings, 80: 3296-3304. https://doi.org/10.1016/j.matpr.2021.07.240
- [15] Salman, H.H., Ali, M.A.M., Ali, E.T. (2020). Synthesis and screening of anticancer potentials of some new terephthaldehyde-derived nitrone compounds. Tropical Journal of Pharmaceutical Research, 19(2): 341-349. https://doi.org/10.4314/tjpr.v19i2.17
- [16] Sharma, R., Acharya, A.D., Shrivastava, S.B., Shripathi, T., Ganesan, V. (2014). Preparation and characterization of transparent NiO thin films deposited by spray pyrolysis technique. Optik, 125(22): 6751-6756. https://doi.org/10.1016/j.ijleo.2014.07.104
- [17] Patil, V., Joshi, P., Chougule, M., Sen, S. (2011). Synthesis and characterization of Co3O4 thin film. Soft Nanoscience Letters, 2(1): 1-7. http://doi.org/10.4236/snl.2012.21001
- [18] Jalili, S., Hajakbari, F., Hojabri, A. (2018). Effect of silver thickness on structural, optical and morphological properties of nanocrystalline Ag/NiO thin films. Journal of Theoretical and Applied Physics, 12(1): 15-22. https://doi.org/10.1007/s40094-018-0275-2
- [19] Mohammed, H.R.A., Hasan, N.B., Shinen, M.H. (2025). Structural, morphological and optical properties of (NiO)_{1-x}(Co₃O₄)_x composite thin films prepared by chemical spray pyrolysis technique. Revue des Composites et des Matériaux Avancés, 35(2): 367. https://doi.org/10.18280/rcma.350218
- [20] Abbas, S.Z., Aboud, A.A., Irfan, M., Alam, S. (2014). Effect of substrate temperature on structure and optical properties of Co₃O₄ films prepared by spray pyrolysis technique. IOP Conference Series: Materials Science and Engineering: 60(1): 012058. https://doi.org/10.1088/1757-899X/60/1/012058
- [21] Shammary, N.F.A. (2010). Optical characteristics of NiO thin film on glass formed by chemical spray pyrolysis. Journal of kufa-Physics, 2(1): 22-27.
- [22] Abass, K.H., Shinen, M.H., Alkaim, A.F. (2018).

 Preparation of TiO2 nanolayers via sol-gel method and study the optoelectronic properties as solar cell application. Journal of Engineering and Applied Sciences, 13(22): 9631-9637. https://doi.org/10.3233/AJW230062

- [23] AlSultani, M.J., Alias, M.F.A. (2025). Impact of graphene oxide concentration and anthocyanin dye on the structural, morphological and optical properties of GO: TiO2 thin films. Iraqi Journal of Science, 66(6): 2336-2349. https://doi.org/10.24996/ijs.2025.66.6.12
- [24] Huo, N., Konstantatos, G. (2018). Recent progress and future prospects of 2D-based photodetectors. Advanced Materials, 30(51): 1801164. https://doi.org/10.1002/adma.201801164
- [25] Nallabala, N.K.R., Vattikuti, S.P., Verma, V.K., Singh, V.R., et al. (2022). Highly sensitive and cost-effective metal-semiconductor-metal asymmetric type Schottky metallization based ultraviolet photodetecting sensors fabricated on n-type GaN. Materials Science in Semiconductor Processing, 138: 106297. https://doi.org/10.1016/j.mssp.2021.106297
- [26] Punde, A.L., Shah, S.P., Hase, Y.V., Waghmare, A.D., et al. (2022). Self-biased photodetector using 2D layered bismuth triiodide (BiI 3) prepared using the spin coating method. RSC Advances, 12(46): 30157-30166.

- https://doi.org/10.1039/D2RA05484A
- [27] Liang, G.X., Li, C.H., Zhao, J., Fu, Y., et al. (2023). Self-powered broadband kesterite photodetector with ultrahigh specific detectivity for weak light applications. SusMat, 3(5): 682-696. http://doi.org/10.1002/sus2.160
- [28] Hao, D., Liu, D., Shen, Y., Shi, Q., Huang, J. (2021). Air-stable self-powered photodetectors based on lead-free CsBi3I10/SnO2 heterojunction for weak light detection. Advanced Functional Materials, 31(21): 2100773. https://doi.org/10.1002/adfm.202100773
- [29] Zhang, T.F., Li, Z.P., Wang, J.Z., Kong, W.Y., et al. (2016). Broadband photodetector based on carbon nanotube thin film/single layer graphene Schottky junction. Scientific Reports, 6(1): 38569. https://doi.org/10.1038/srep38569
- [30] Xu, J., Yang, W., Chen, H., Zheng, L., Hu, M., Li, Y., Fang, X. (2018). Efficiency enhancement of TiO2 self-powered UV photodetectors using a transparent Ag nanowire electrode. Journal of Materials Chemistry C, 6(13): 3334-3340. https://doi.org/10.1039/C8TC00550H